

Revisiting the February 6th 1783 Scilla (Calabria, Italy) landslide and tsunami by numerical simulation

P. Mazzanti · F. Bozzano

Received: 7 April 2010/Accepted: 28 January 2011/Published online: 16 February 2011
© Springer Science+Business Media B.V. 2011

Abstract On February 6th, 1783, a landslide of about $5 \times 10^6 \text{ m}^3$ triggered by a 5.8 M earthquake occurred near the village of Scilla (Southern Calabria, Italy). The rock mass fell into the sea as a rock avalanche, producing a tsunami with a run-up as high as 16 m. The tsunami killed about 1,500 people, making it one of the most catastrophic tsunamis in Italian history. A combined landslide-tsunami simulation is proposed in this paper. It is based on an already performed reconstruction of the landslide, derived from subaerial and submarine investigation by means of geomorphological, geological and geomechanical surveys. The DAN3D model is used to simulate the landslide propagation both in the subaerial and in the submerged parts of the slope, while a simple linear shallow water model is applied for both tsunami generation and propagation. A satisfying back-analysis of the landslide propagation has been achieved in terms of run-out, areal distribution and thickness of the final deposit. Moreover, landslide velocities comparable to similar events reported in the literature are achieved. Output data from numerical simulation of the landslide are used as input parameters for tsunami modelling. It is worth noting that locations affected by recordable waves according to the simulation

correspond to those ones recorded by historical documents. With regard to run-up heights a good agreement is achieved at some locations (Messina, Catona, Punta del Faro) between computed and real values, while in other places modelled heights are overestimated. The discrepancies, which were most significant at locations characterized by a very low slope gradient in the vicinity of the landslide, were probably caused by effects such as wave breaking, for which the adopted tsunami model does not account, as well as by uncertainties in the historical data.

Keywords Scilla (Calabria, Italy) · Tsunami · Numerical modelling · Back-analysis · Rock avalanche

Introduction

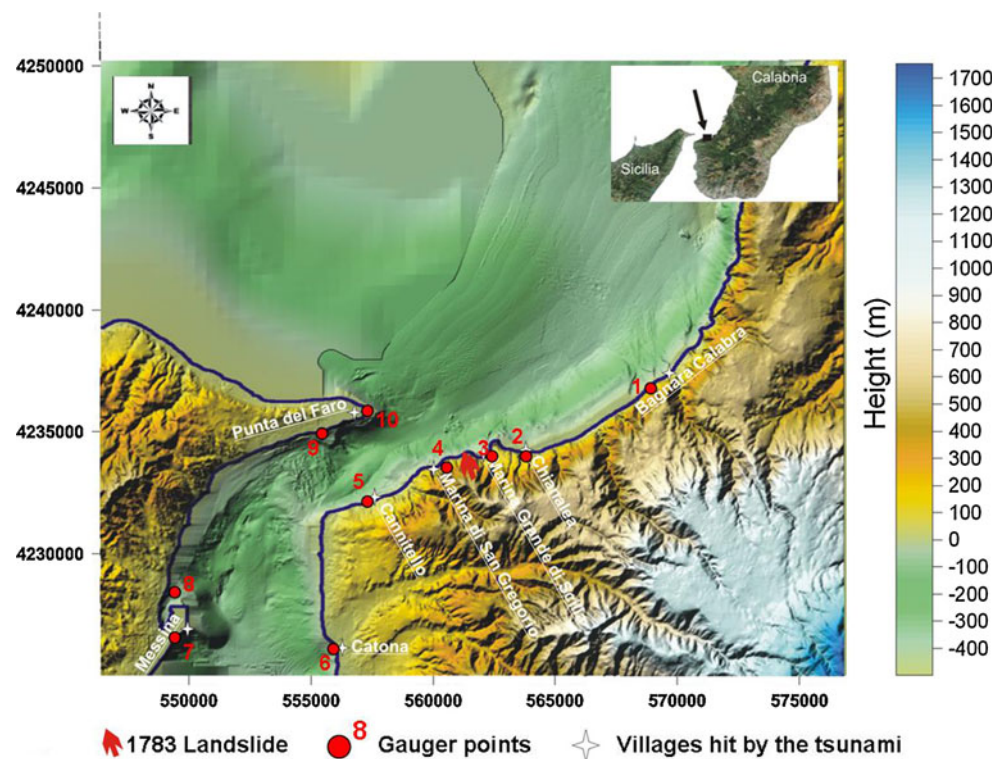
South-eastern Calabria (Italy) is particularly susceptible to natural hazards like earthquakes, landslides and tsunamis, and it has experienced several catastrophic events in historical and pre-historical times (Sarconi 1784; Baratta 1901, 1910; Mercalli 1906). One of the most recent events is the so-called “1783 Terremoto delle Calabrie” earthquake, a seismic sequence characterized by five main shocks between M5.8 and M7.3 that struck the southern part of Calabria between February 5th and March 28th 1783. The number of casualties, already high because of the earthquake, rose further due to seismic-induced phenomena such as landslides that are well described in the historical sources (Minasi 1785). One of the largest landslides occurred 30 min after the February 6th earthquake (immediately after midnight) south of Scilla (Fig. 1) and, plunging into the sea, induced a huge tsunami, as high as 16 m, that killed more than 1,500 inhabitants along the Marina Grande beach (Hamilton 1783; Sarconi 1784;

P. Mazzanti (✉) · F. Bozzano
Dipartimento di Scienze della Terra, “Sapienza” Università di Roma, P.le Aldo Moro, 5, 00185 Rome, Italy
e-mail: paolo.mazzanti@uniroma1.it

P. Mazzanti · F. Bozzano
NHAZCA S.r.l., spin-off “Sapienza” Università di Roma, Via Cori s.n.c., 00177 Rome, Italy

F. Bozzano
CERI Research Centre “Prediction, Prevention and Mitigation of Geological Risks”, Università di Roma “Sapienza”, Piazza U. Pilozzi, 9, Viale Montesacro, 00177 Rome, Italy

Fig. 1 DTMM (Digital Terrain and Marine Model) of Southern Calabria and the sector of Sicily overlooking the Messina Straits with indicated the location of the 1783 Scilla landslide, the villages affected by the Tsunami and the gauge points used in the tsunami simulation



Minasi 1785; Vivenzio 1788; De Lorenzo 1877). Given the large number of casualties, this event can be considered one of the most catastrophic landslide-induced tsunami historically documented in Italy, as already stated by the Italian Tsunami Catalogue (Tinti et al. 2007).

This coastal landslide was recently analyzed by means of both subaerial and submarine surveys (Bozzano et al. 2008; Mazzanti 2008a, b). In particular, a dedicated sonar multibeam survey was performed in the frame of the PRIN Italian National Project “Integration of inshore and offshore geological and geophysical innovative techniques for coastal landslides studies” (Principal Investigator: F.L. Chiocci). The high resolution bathymetry allowed to recognize and map a huge submarine deposit just in front of the subaerial landslide as well as a large submarine scar. Starting from these accurate data the 6th February 1783 catastrophic events were critically revisited by simple numerical codes for the simulation of both landslide propagation and tsunami. A combined numerical back analysis of the landslide and tsunami was performed aiming to achieve the best fitting between the real event and the simulated one. Landslide features (e.g. initial volume, run-out, deposit distribution) were used as fixed values in the numerical back analysis, thus obtaining information about landslide velocity and thickness during the propagation. Then, these values were used as input data for the tsunami simulation. These numerical results, compared to field evidences and historical witnesses, allowed to infer new insights into the overall events occurred on the 6th

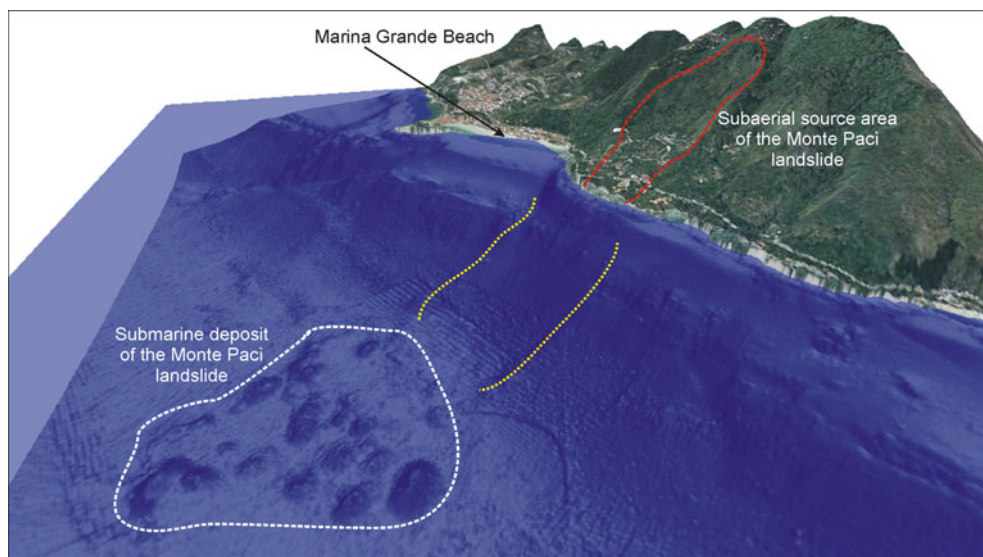
February 1783. Furthermore, the validation and calibration of these numerical models and approaches on a well known past event can be seen as a key step in the forecasting analysis of risks related to landslide induced tsunamis, especially in an area like the Southern Calabria (Italy) which is particularly susceptible to geological hazards.

The 6th February 1783 Scilla landslide

The Scilla coastal landslide occurred on February 6th 1783 close to the village of Scilla and was triggered by the second main shock of the “Terremoto delle Calabrie” seismic sequence (Boschi et al. 2000). Extensive studies have been carried out in both the subaerial and the submarine parts of the slope in order to characterize the landslide (Bosman et al. 2006; Bozzano et al. 2008). In what follows, the main results of submarine and subaerial investigations (Bozzano et al. 2010; Mazzanti 2008a, b), which are relevant to the numerical analysis, are summarized by looking at the overall slope.

The phenomenon affected the M. Paci slope (Fig. 2), where a large subaerial depression is still visible. The slope is quite steep (up to 45°) and intensely jointed gneiss rock and breccias crop out extensively (Bozzano et al. 2008, 2010; Mazzanti 2008a, b). The landslide was bounded by two faults in the upper and lower part of the scar area and laterally confined (in the left flank) by a major regional fault (Monte Paci Fault). This geological and structural

Fig. 2 3D perspective view of the Scilla coastal sector. The white dashed line bounds the 1783 landslide deposit. The red dashed line encloses the subaerial landslide. The yellow dotted lines identify the lateral boundaries of the submarine depression



conditions of the Monte Paci slope represented both a predisposing factor and a kinematic control for the 1783 Scilla landslide. In particular, it is suggested the failure of a wedge of rock which then evolved into a rock avalanche due to the fragmentation of the intensely jointed rock-mass and to the slope morphology (Bozzano et al. 2008, 2010; Mazzanti 2008a, b).

The subaerial volume mobilized during the February 6th landslide has been calculated as the difference between a hypothetical pre-landslide morphology and the present morphology of the slope; the original morphology was achieved by reshaping the slope based on both key geomorphological features and engravings by A. Minasi (1970). The achieved volume is on the order of $5.4 \times 10^6 \text{ m}^3$.

The results of submarine geophysical investigations (Bosman et al. 2006) allowed for recognition of a large submarine depression just at the toe of the subaerial scar (Fig. 2). Furthermore, a huge depositional bulge with a hummocky morphology (Fig. 2) was identified just at the toe of the submarine depression, and it has been interpreted as the landslide deposit. The maximum thickness of the deposit, estimated by considering both geomorphological features (from high resolution bathymetry) and Sparker seismic profiles (Bosman et al. 2006), is about 15 m. Furthermore, large blocks have been detected within the deposit, each accounting for a volume between 100 and 200,000 m^3 (Mazzanti 2008a, b). These blocks are randomly distributed in the deposit without any volume-to-travel-distance rules, and they reached a maximum distance of 1.7 km from the coastline. The landslide accumulation (Fig. 2) is widely spread over a relatively flat seafloor and covers an area of about 1 km^2 . Despite the difficulty in its estimation, the total volume of the deposit seems comparable to the subaerial landslide volume of $5.4 \times 10^6 \text{ m}^3$.

Analyses of the correlation between the subaerial and submarine depression suggest that they occurred as two separate events (Mazzanti 2008b). As a matter of fact, morphological evidences inferred by HR Multibeam Bathymetry in the conjunction zone between the subaerial and the submarine scars (i.e. the head of the submarine scar visible only from 100 m below the sea level, the smooth face of the scarp, the “progradation” of the coast after the landslide described in historical documents and the presence of a sea level standing platform at about 90 m below the sea level) suggest that the submarine landslide occurred before the 1783. Hence, only the subaerial landslide is considered in the present paper as the source of the February 6th 1783 tsunami at Scilla.

The February 6th 1783 tsunami

It is widely accepted in the scientific literature that the February 6th tsunami at Scilla was induced by the M. Paci landslide (Tinti and Guidoboni 1988; Tinti et al. 2004; Graziani et al. 2006; Gerardi et al. 2008). The time sequence of the earthquake, landslide and tsunami can be seen as the first clear evidence of a landslide source for the tsunami. As a matter of fact, according to historical reconstructions, the landslide occurred about 30 min after the earthquake, and the tsunami hit the adjacent Marina Grande beach 30–60 s after the landslide. Moreover, both the limited area around Scilla affected by the wave and the corresponding wave height distribution confirm the landslide origin of the tsunami (Okal and Synolakis 2004; Gerardi et al. 2008). Maximum run-up heights ranging from 6 to 9 m according to Sarconi (1784) and up to 16 m according to Minasi (1785) were recorded along the Marina Grande beach. In the Calabrian coastal sector between Nicotera and Reggio Calabria,

Table 1 Inundation distance and run-up height in some of the locations along the coast

Site	Inundation distance (m)	Run-up height (m)
Bagnara Calabria	n.a.	n.a.
Cannitello	50 (r)	0.8–2.9 (c)
Catona	10 (r)	0.3–0.7 (c)
Chianalea	n.a.	5–6
Marina Grande (Scilla)	n.a.	9–16 (r)
Marina San Gregorio	n.a.	n.a.
Messina	50 (r)	2 (r)
Punta del Faro	400 (r)	6–13 (c)

r Historically reported, c Computed from the reported inundation distance (Gerardi et al. 2008), n.a. data not available

as well as along the Sicilian coast, several towns and villages, such as Cannitello, Bagnara Calabria, Punta del Faro, and Messina, were hit by the wave (Fig. 1). As one can see in Table 1, however, the wave run-up height and the inundation distance (based on historical documents) drastically decrease moving away from Scilla.

Numerical modelling of the landslide propagation

The numerical models

The post-failure propagation of the Scilla landslide was modelled using the three dimensional DAN3D code (McDougall and Hungr 2004). DAN3D (Hungr and McDougall 2009) is one of the most powerful codes for the numerical modelling of subaerial landslide and in the last years has been tested and calibrated over several real cases (e.g. McDougall et al. 2006; Sosio et al. 2008; Evans et al. 2009). The main features of the DAN3D code are listed below.

- (1) The material is considered as an “equivalent fluid” (Hungr 1995), governed by simple rheological relationships (McDougall and Hungr 2004; Hungr and McDougall 2009) that can vary along the path of motion according to the characteristics of the landslide material.
- (2) The model considers strain-dependent, non-hydrostatic, anisotropic internal stresses due to the 3D deformation of material with internal shear strength and centripetal acceleration due to path curvature.
- (3) The model simulates mass and momentum transfer due to entrainment of material and allows for the consideration of corresponding changes in flow rheology along the path.

The depth-integrated St. Venant equations are solved using a Lagrangian numerical method adapted from smoothed particle hydrodynamics (Monaghan 1992). The momentum

equations consider a fixed frictional internal rheology governed by an internal friction angle and a user-selected basal rheology, as provided by several alternative rheological kernels (Hungr 1995). The rheology is determined by one or two parameters (depending on the selected rheology) which must be adjusted by a trial-and-error calibration procedure performed by back-analyzing recorded events.

Although the code was specifically designed to simulate the dynamics of subaerial landslides, it has been previously applied to other submarine and coastal mass movements by using the equivalent fluid equivalent medium approach (Mazzanti et al. 2009; Mazzanti and Bozzano 2009). By this approach, extensively described in Mazzanti and Bozzano (2009), the following basic aspects must be accounted for in the numerical simulation of coastal landslides: 1) the buoyancy effect; 2) drag forces; 3) peculiar mechanisms like hydroplaning (Mohrig et al. 1998), and 4) the sudden change of environment (water impact) which can produce an impulsive loss of energy and several modifications in the flow behaviour.

Input data

The 1783 Scilla landslide was simulated using a DTMM (Digital Terrain and Marine Model) with 20 m square cells (Fig. 3), obtained by combining subaerial DTM (based on a 1:5,000 topographic map) and high resolution bathymetry collected by sonar multibeam surveys (Bosman et al. 2006; Mazzanti 2008a, b). A detached volume of $5.4 \times 10^6 \text{ m}^3$ and a maximum run-out of 2.5 km from the upper scar were considered in the numerical back-analysis. A sensitivity analysis was performed in order to define the best rheological parameters for the simulation (Table 2).

The use of frictional rheology in the subaerial part of the slope is reasonable if we assume that the slope was affected by a rock slide-type landslide and that after the failure the landslide mass was fragmented and became a rock avalanche (Bozzano et al. 2008; Mazzanti 2008b). A dynamic friction angle of 16° is common for such a landslide in the subaerial (e.g. Hungr and Evans 1996; review in Sosio et al. 2008; Pirulli and Mangeney 2008) and submarine (e.g. Mangeney et al. 2000) environment. Along the submarine path, the Voellmy rheology (Hungr 1995) was used with a dry friction coefficient $\mu = 0.05$ and a turbulence coefficient $\xi = 220 \text{ m/s}^2$. The turbulence coefficient accounts in a fictitious way for either the inner turbulence effects in the landslide’s mass (assumed as an equivalent fluid) or for the drag forces that are due to the interaction of the moving mass with the surrounding water. Erosion of the moving mass along the pathway was set to zero since no data were available at this regard and it is reasonable to assume that a small thickness of erodible debris could be present along the landslide pathway.

Fig. 3 Aerial view and present multibeam bathymetry (left) and pre-landslide 50 m DTMM (right) used in the landslide modelling

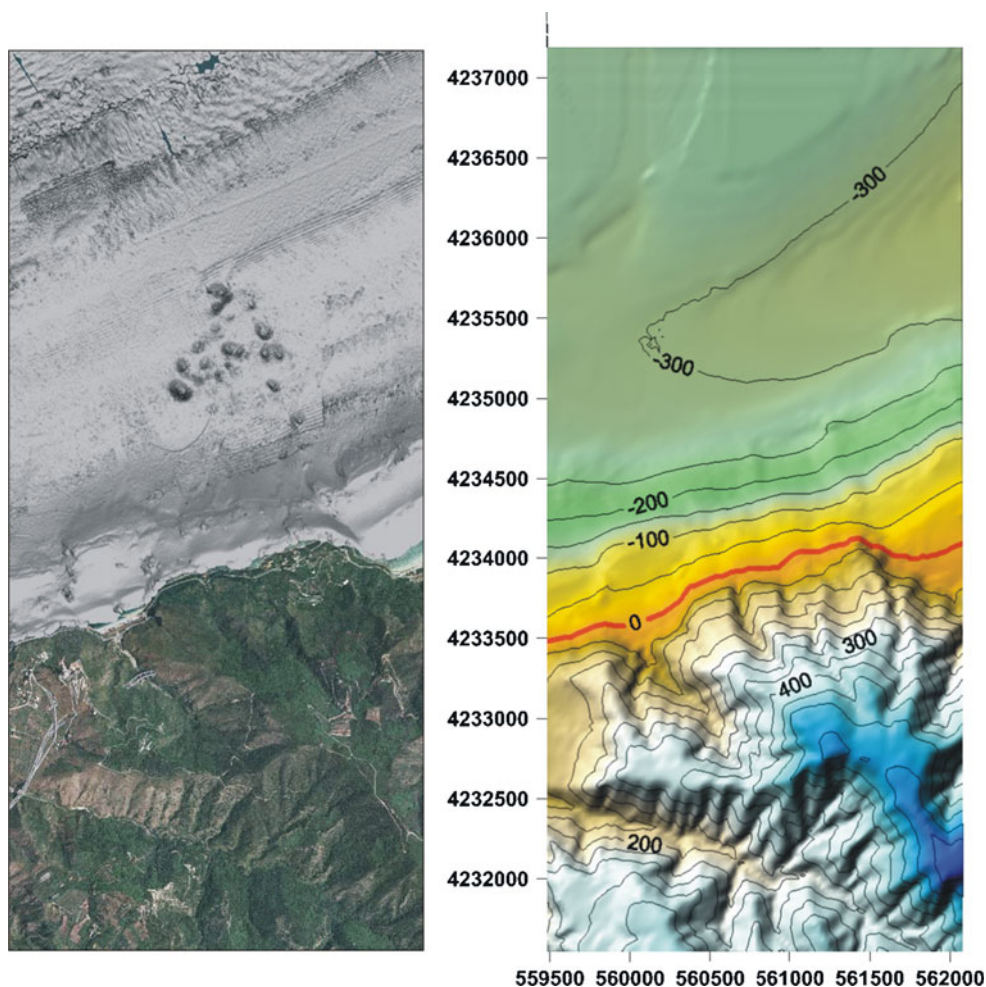


Table 2 Parameters used in the best simulation of the Scilla rock avalanche by DAN3D

Subaerial rheology	Frictional
Unit weight (kN/m^3)	17
Friction angle ($^\circ$)	16
Erosion (m)	0
Subaqueous rheology	Voellmy
Unit weight (kN/m^3)	17
Friction coefficient (μ)	0.05
Turbulence coefficient (ζ) (m/s^2)	220
Erosion (m)	0

Simulation results

The simulation results (Fig. 4) show that the mass reaches the flat area in front of Scilla after about 40 s and the final run-out after 80 s; in the following 40 s (from 80 to 120 s), only a lateral spreading of the material is observed. Figure 4 shows the agreement between the computed and recorded run-out and the areal distribution of the final deposit.

A maximum landslide velocity of 45 m/s is reached about 15–20 s (Fig. 5) after the failure in the frontal part of the mass (in the submarine slope). Then, the moving mass maintains a velocity greater than 40 m/s until 30 s that decreases below 20 m/s after 60 s from the collapse. After 70–80 s, the mass moves at a rate lower than 10 m/s.

Historical documents testify to an intense 30 s long noise coming from Monte Pacì before the arrival of the tsunami (Minasi 1785). This noise can be interpreted as the result of the slope failure in the elapsed time between landslide detachment and its complete submergence. This time (also accounting for the uncertainties in the historical report) is comparable to the subaerial propagation period computed by the numerical simulation. Unfortunately, no historical data are available regarding the landslide velocity. Nevertheless, the computed values are in accordance with those proposed in the literature for similar landslides (Sosio et al. 2008; Locat et al. 2004). Figure 6 shows time series of the thickness in the first 42 s of the simulation. The thickness is reduced from the initial value (higher than 60 m) down to 40 m during the first 18 s and between 20 and 25 m in the submarine slope during the first 42 s. These thickness values

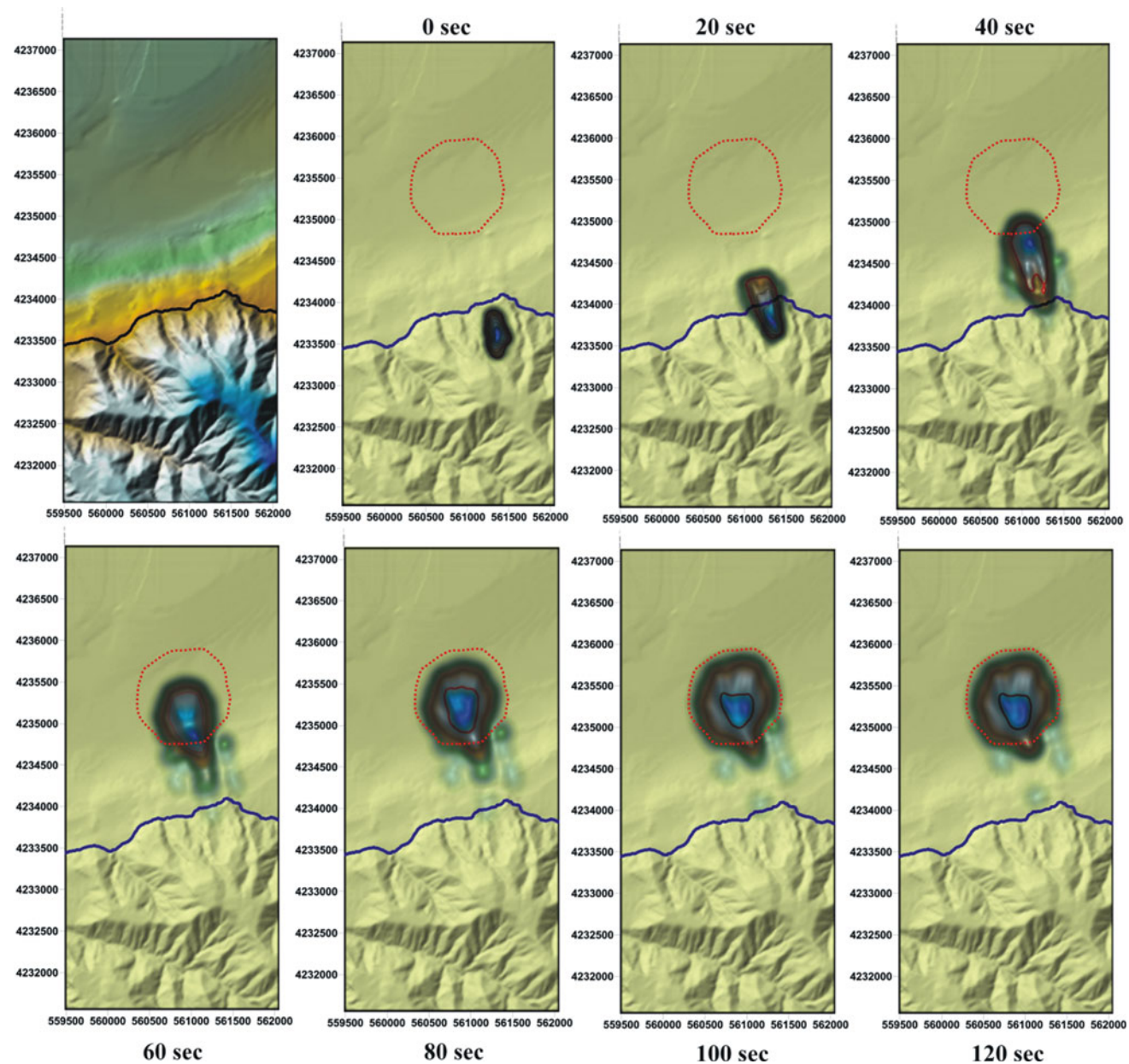


Fig. 4 Time sequence of the landslide propagation (plan view). The red dotted line bounds the real mapped landslide deposit

refer to the frontal part of the moving mass. A similar behavior has also been observed for the velocity (Fig. 5); in this case, the highest values were recorded just behind the frontal part of the moving mass.

Froude number analysis

Tsunamis generated by rock slides and rock avalanches are determined by the volume, shape, velocity profile and run-out length of the landslide for a given bathymetry. The Froude number is given by the ratio of the landslide speed (v) to the linear long-wave speed, \sqrt{gh} ,

$$\text{Fr} = \frac{v}{\sqrt{gh}}, \quad (1)$$

where g is the acceleration of gravity, and h is the water depth (Harbitz et al. 2006). Sub-critical, critical and super-critical landslide velocities are defined as $\text{Fr} < 1$, $\text{Fr} \approx 1$ and $\text{Fr} > 1$, respectively. Sub-critical landslide velocities imply that the generated waves will propagate ahead of the moving landslide, and, correspondingly, for super-critical landslide velocities, the landslide will move faster than the waves and goes ahead. For both cases, the build-up of the wave is limited. The most efficient generation is when the landslide velocity and tsunami velocity are similar, i.e.

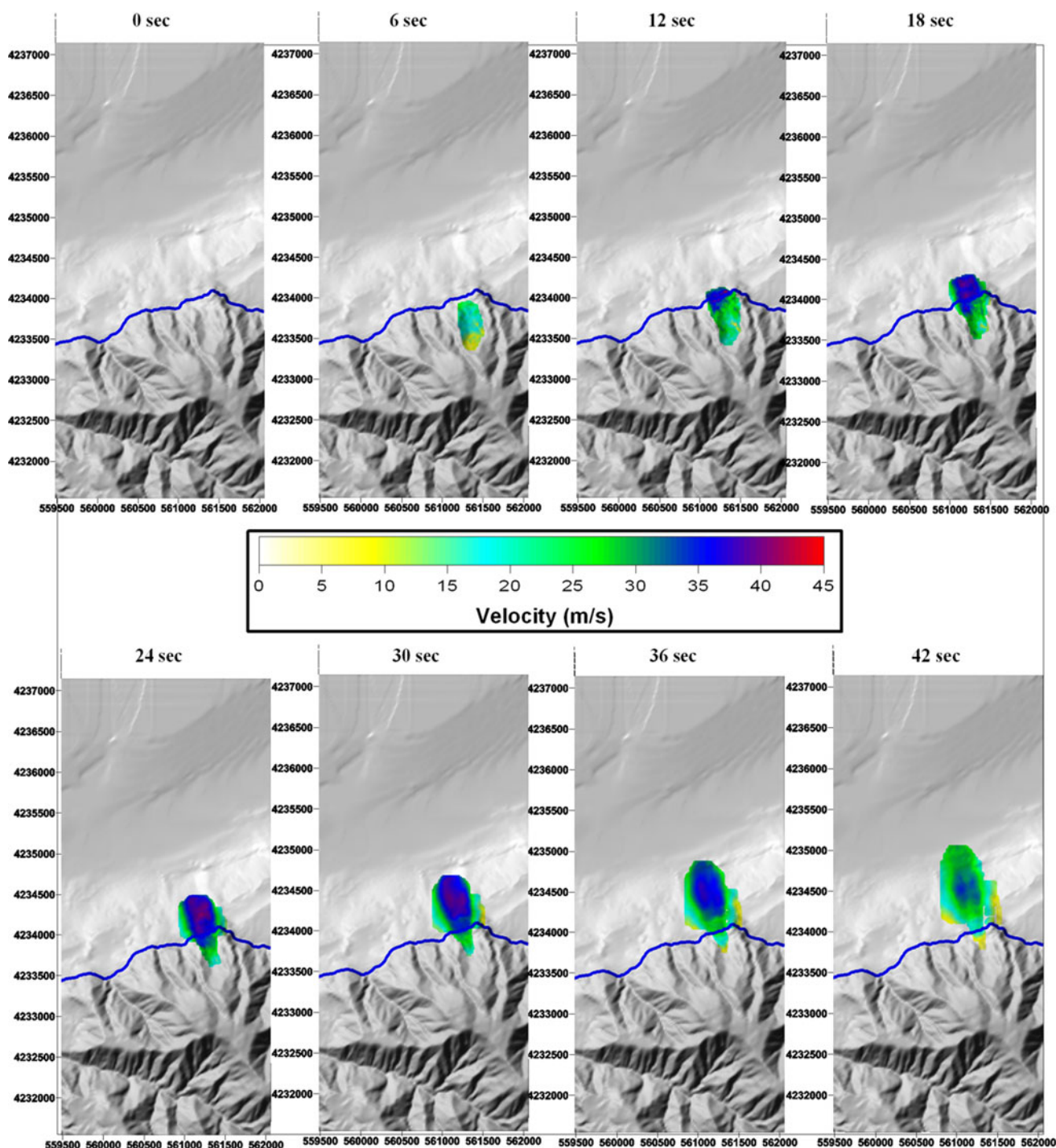


Fig. 5 Time sequence of the landslide velocity distribution during the first 42 s of numerical simulation

when the Froude number is close to 1. During the travel down the slope, the Froude number varies along the path due to the change in landslide velocity and the change in water depth, which again leads to a change in wave speed.

The Froude number along the submerged path of the Scilla landslide was computed based on the results of the landslide simulation performed by DAN3D in two

horizontal dimensions (Fig. 7). Critical and supercritical values were computed until 60 s after the start of the landslide. During the overall landslide propagation, critical values were computed from the coastline to 600 m in the nearshore. The highest values of the Froude number (up to 3.3) were computed in the shallow water close to the coastline until 45 s after the start of the landslide.

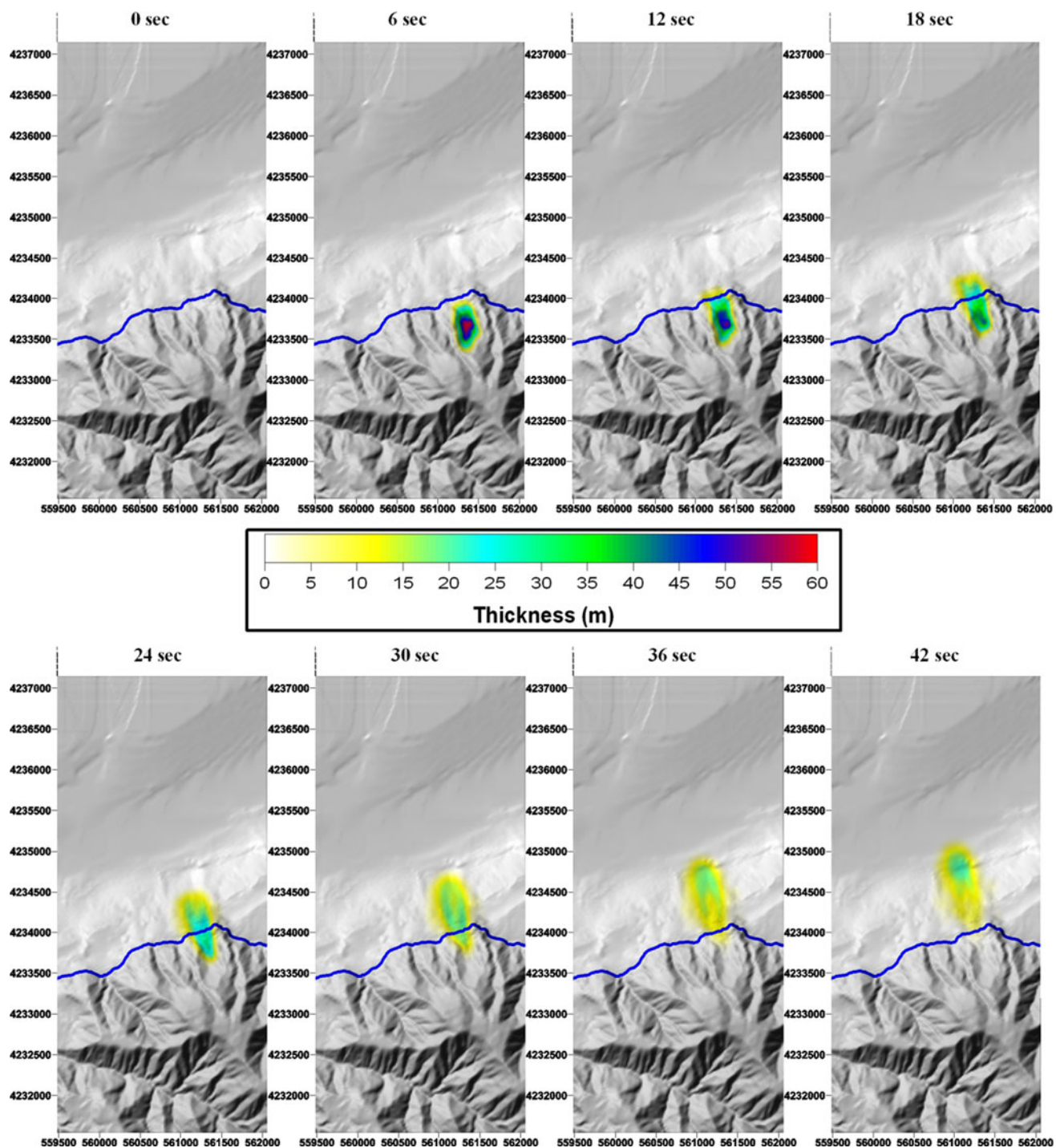


Fig. 6 Time sequence of the landslide thickness distribution during the first 42 s of numerical simulation

From the Froude number analysis (Fig. 7), the high tsunamigenic potential of the Scilla landslide can be inferred. In the first 600 m of the submarine path, Froude numbers close to the critical value are maintained in the frontal part of the mass, thus resulting in a significant tsunamigenic potential. The Froude number analysis was also useful in establishing the best value of landslide thickness (i.e. 25 m) during the sliding for use in the

tsunami model. The frontal landslide thickness corresponding to a Froude number close to the critical value was considered a representative value for the height of a non-deformable block which will be used in the tsunami generation model. As a matter of fact, the achieved values of 20–25 m are very close to the mean value of the landslide thickness during the underwater propagation (Fig. 6).

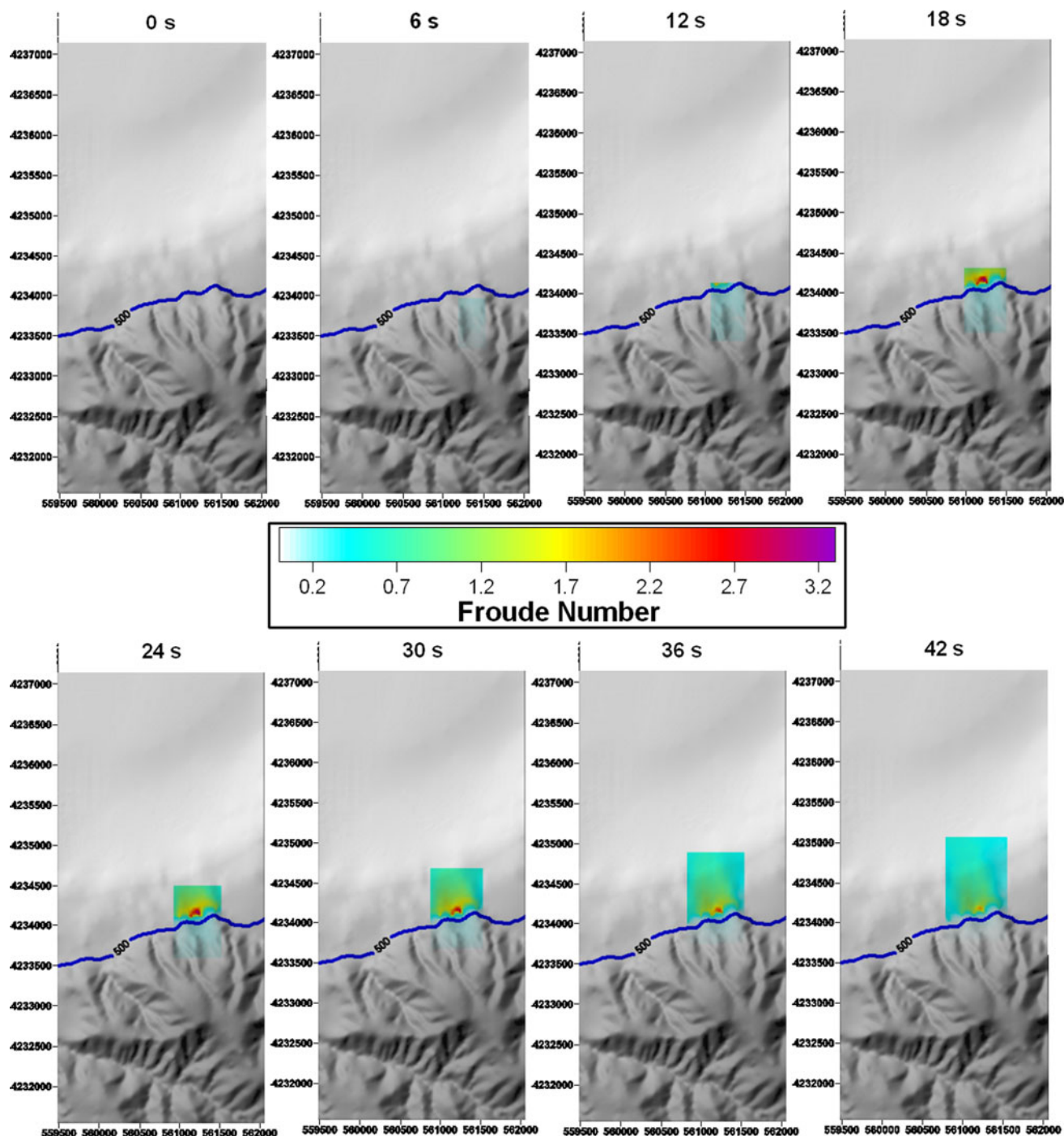


Fig. 7 Time sequence of the 3D Froude number distribution during the first 42 s of numerical simulation

Numerical modelling of the tsunami

The numerical models

Numerical modelling of the 1783 Scilla tsunami was performed with a linear shallow water model, which was applied to both tsunami generation and propagation as described by Harbitz and Pedersen (1992). In this model, the landslide is

simplified and described as a flexible box with a pre-defined velocity progression. The dimensions of the box are defined by the physical extensions of the slide and are given as input to the numerical model (length, width, and height). The box is rounded to avoid numerical noise due to sharp edges, and the landslide propagation follows a straight line. The travel distance of the slide $s(t)$ at time t describes an acceleration phase, a constant speed phase, and a deceleration phase:

Acceleration phase:

$$s(t) = R_a \left(1 - \cos \left(\frac{U_m}{R_a} t \right) \right), \quad 0 < t < T_a \quad (2)$$

Constant speed phase:

$$s(t) = R_a + U_m(t - T_a), \quad T_a < t < T_c + T_a \quad (3)$$

Deceleration phase:

$$s(t) = R_a + R_c + R_d \sin \left(\frac{U_m}{R_d} (t - T_a - T_c) \right), \quad T_c + T_a < t < T_a + T_c + T_d \quad (4)$$

where U_m is the maximum slide velocity, T_a is the acceleration time, R_a is the acceleration distance, T_c is the constant speed time, R_c is the constant speed distance, T_d is the deceleration time, and R_d is the deceleration distance. The total travel time is $T = T_a + T_c + T_d$, while the run-out distance of the slide is $R = R_a + R_c + R_d$. Further details on the landslide representation can be found in Harbitz (1992) and Løvholt et al. (2005). The model is validated among others against observations of the catastrophic 1934 Tafjord rock slide tsunami event, Western Norway (Harbitz et al. 1993).

Input data

The following input data were used in the tsunami simulation based on the available dataset and the aforementioned analyses (Table 3). The DTMM (Digital Terrain and Marine Model), achieved by combining high resolution multibeam bathymetry with a grid spacing of 20 m in the nearshore (merged with a 100 m-grid bathymetry in the offshore) has been used as the topography for the simulation.

Landslide propagation features have been inferred by detailed field surveys, geophysical landslide investigations and in particular by the landslide numerical simulation. Specifically, in order to apply the simplified tsunami model to the 1783 Scilla landslide, the 3D landslide geometry during the propagation achieved by DAN3D simulation (Fig. 6) have been converted into a non-deformable block

(Fig. 8), the size and thickness of which were as representative as possible for the simulated landslide geometry during the early stages of the submerged propagation (the most important phases in the tsunami generation). With regard to the velocity a simplified profile with a constant acceleration phase, a constant velocity phase and a constant deceleration phase has to be achieved from the landslide simulation performed by DAN3D (Fig. 5); this profile should represent the best approximation of the simulated landslide velocity distribution for tsunami modelling purposes (Fig. 8). Furthermore, the Froude number analysis described above, was also performed with the aim of achieving a combination of thickness and velocity so that the non-deformable block had the “equivalent” tsunami-generative power as the simulated landslide (i.e. the thickness and velocity should be comparable over the time of critical Froude number conditions).

Simulation results

Simulation results consist of 2D maps of the wave distribution in the investigated area and time series of wave elevation over time at specific points (gauge points) which are showed in Fig. 1. For each location there are three gauge points (at depths of 100, 50 and 20 m) in order to monitor the amplification of the wave towards the coast. The perimeters of the landslide at the start- and end-positions are drawn in yellow and white, respectively. Figure 9 shows pictures of the surface elevation after 2, 5 and 10 min, while Fig. 10 shows the maximum surface elevation during the first 20 min of simulation. The wave front starts to propagate radially from the landslide, with the highest waves in the sliding direction, i.e. perpendicular to the coast of Scilla. After 5 min the wave front reaches the NE Sicily coast, and it moves along the coast of Calabria and Sicily. After 10 min the wave front approaches Bagnara Calabria, north of Scilla, (Fig. 1) and enters in the Messina Straits. One can observe reflection, refraction and interference effects in the wave pattern. The surface elevation in open water is about 6–8 m (Fig. 9).

Table 3 The landslide features used in the tsunami modelling

Landslide geometry				
Length (m)	Width (m)	Height (m)	Assumed volume ^a ($10^6 \times m^3$)	
700	280	25	5.4	
Landslide dynamics				
Acceleration length (m)	Constant speed length (m)	Retardation length (m)	Max. velocity (m/s)	Run-out distance (m)
350	350	1,000	45	1,700

^a The volume of the landslide is slightly larger than the product of length, width, and height owing to a rounding of the slide box to avoid numerical instabilities

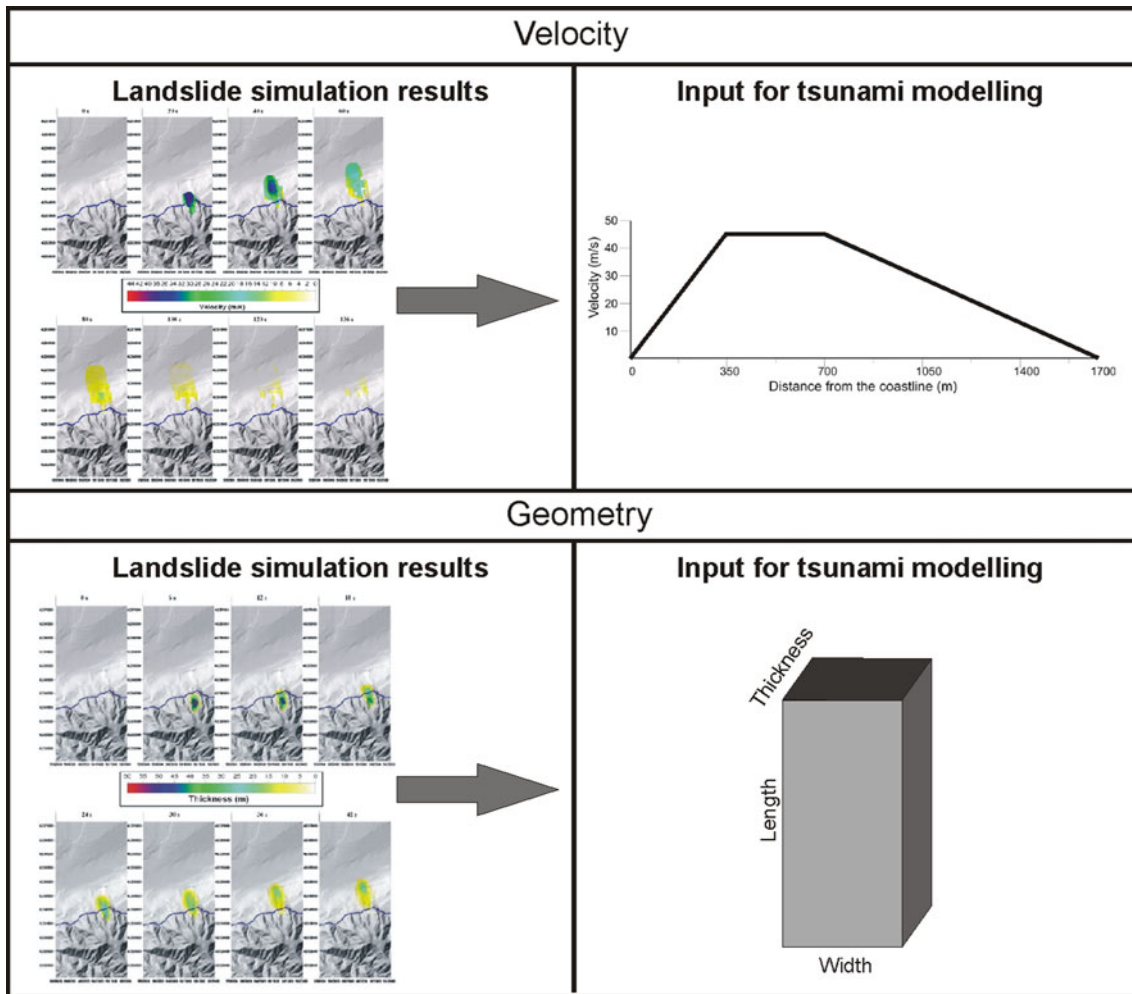


Fig. 8 Sketch explaining how the landslide simulation results (in terms of velocity and geometry) are converted in order to be used as input parameters for the tsunami modelling (see text for details)

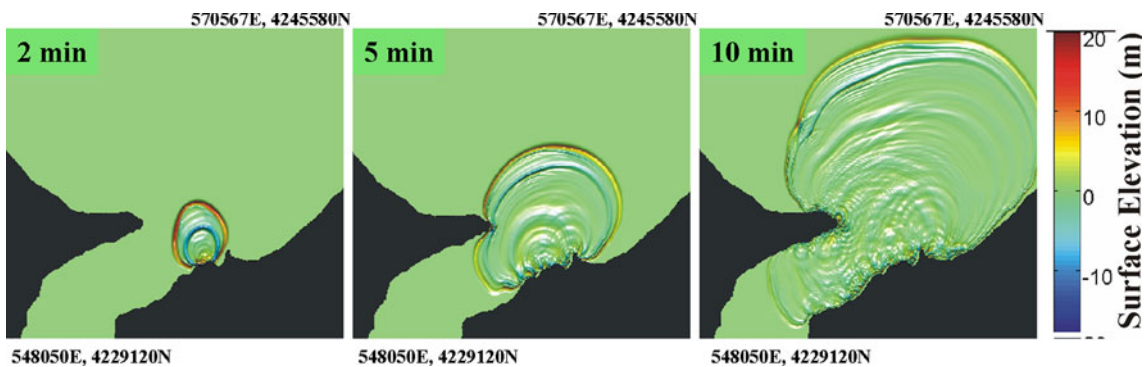


Fig. 9 Time sequence of the wave surface elevation during the first 10 min after the landslide occurrence

The run-up values at the coastline were determined by using the simulated surface elevation of the highest wave of the leading part of the wave train. Here, the surface elevation at a depth of 100 m (before the wave starts to amplify due to shoaling) was used in the run-up

calculations. Based on the run-up factors of nonlinear waves found in laboratory experiments (Pedersen and Gjevik 1983), the run-up was determined by multiplying the measured surface elevation with these factors. The factor chosen depends on the bathymetric slope and varies

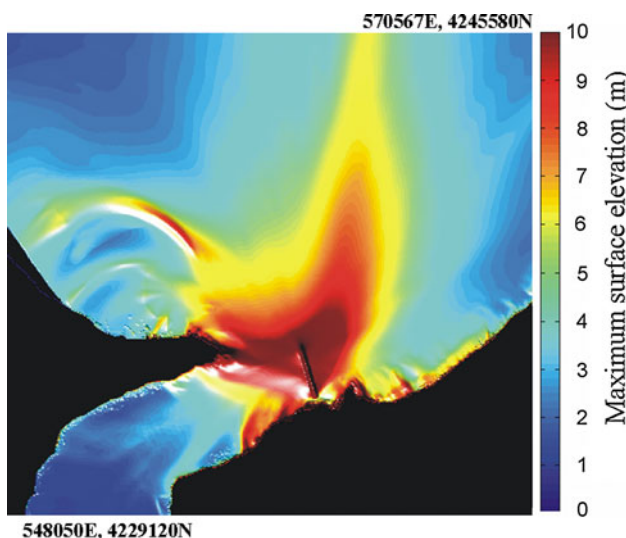


Fig. 10 Maximum surface elevation of the wave during the first 20 min after the slide. Values higher than 10 m are reported as the dark red color

from 2 (vertical slopes) to 5 (extreme cases with gentle slopes). The bathymetric slopes offshore the selected locations (Fig. 1) are characterized by average inclination angles from 100 m of depth to the coastline from 6° to 19° (Table 4). The factors were reduced for locations close to the landslide, where the amplification was weaker due to waves propagating more parallel to the shoreline (NGI 2008). In particular, for the location Punta del Faro 2, where a low-gradient slope is present from the coast to about 20 m water depth, the factor was further reduced since the model overestimates the waves in the areas in front of the slide for slides moving with such high velocities (NGI 2008). Estimates of run-up heights for the prescribed landslide volumes and velocity profiles are presented in Table 4 where the estimated values of the run-

up height for each location are given as intervals to reflect the uncertainty in the calculation procedures.

Discussion

Comparing the wave run-up reported in historical documents (Table 1) and the values computed by the numerical simulation (Table 4; Fig. 11), a good correspondence in some locations, like Messina (1 and 2), Catona, Punta del Faro, can be seen. In contrast, in other locations, such as Marina di Scilla, Cannitello, Punta del Faro 2 and Chianalea, the computed values overestimate the wave run-up documented in historical documents. The discrepancy could principally be related to the linear shallow water model used for the tsunami, which generally overestimates the run-up values (NGI 2008). The model ignores the effects of dispersion and wave breaking. Wave breaking is especially pronounced for locations with high run-up values and shallow water outside the coastline. If wave breaking occurs, it reduces the run-up height. As a matter of fact, higher discrepancies are recorded in the locations characterized by gentle slopes and high run-up values (Table 4). This explanation is corroborated by the difference between the two gauge points at Punta del Faro (Table 4; Fig. 11): for Punta del Faro1, where the average inclination angle from 100 m depth to the coastline is around 16°, the simulated value and the observed one are comparable; on the contrary, for the Punta del Faro2, where the average inclination angle is significantly lower (8.1°), the simulated value significantly overestimates the observed one. Moreover, uncertainty in the historical data must also be considered as an additional source of error leading to discrepancy between computed and documented values of run-up.

Table 4 Run-up estimates for the locations in the study (see Fig. 1 for locations ID)

Location ID	Location	Average inclination angle from 100 m depth (°)	Computed run-up interval (m)	Historically reported run-up interval (m)
8	Messina	19.1	1–2	2
7	Messina 2	6.7	2–3	2
6	Catona	9.0	About 1	0.3–0.7
3	Marina di Scilla	8.7	25–35	9–16
4	Marina San Gregorio	10.0	25–35	
5	Cannitello	12.9	6–8	0.8–2.9
1	Bagnara Calabria	8.2	7–9	
9	Punta del Faro	16.1	10–15	6–13
10	Punta del Faro 2	8.1	25–40	6–13
2	Chianalea	6.3	15–20	5–6

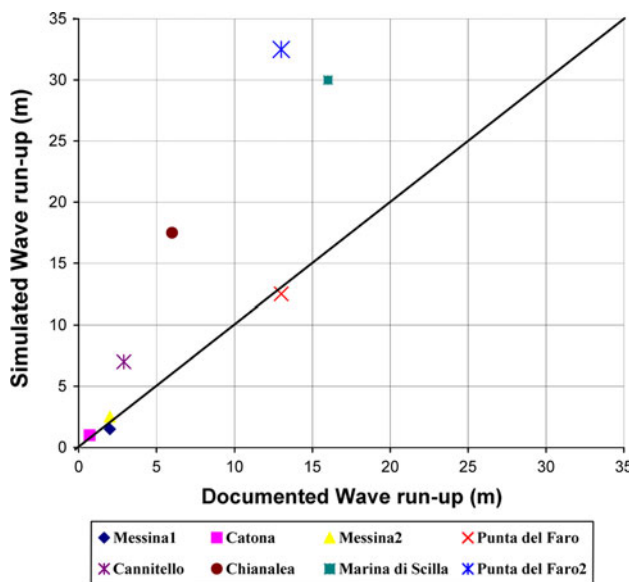


Fig. 11 Documented run-ups versus simulated run-ups for selected gauge point locations

Conclusion

The February 6th 1783 landslide and tsunami at Scilla have been back-analyzed by means of a combined numerical approach. Extensive subaerial and submerged investigations and previous studies (Bosman et al. 2006; Bozzano et al. 2008; Mazzanti 2008a, b), allowed us to define main parameters relevant to the landslide in terms of location, volume, geometry, involved material, and propagation as well as final run-out and deposit distribution. Numerical back-analysis of the landslide propagation was performed by means of the DAN3D model, suitably adapted for the simulation of a combined subaerial-submarine rock avalanche type landslide. Simulation results fit quite well with the recorded event in terms of landslide run-out and final deposit areal distribution and thickness. Furthermore, computed values of landslide velocity are in accordance with values proposed in the literature for similar landslides, thus supporting the overall reliability of the simulation. Then, output data coming from the landslide analysis and numerical modelling (size and geometry, velocity distribution, run-out) were used as input parameters for the tsunami simulation. The tsunami modelling was carried out with a linear shallow water model that describes the landslide as a non-deformable block. Owing to the simplified tsunami model, specific Froude Number analyses were carried out, based on the landslide simulation results to infer, in turn, the most reliable values of landslide parameters to be used in the tsunami modelling. With regard to the estimated run-up heights a good correspondence with values gathered from historical documents was achieved in some locations, while some others were

overestimated. This overestimation is probably due to simplifications of the tsunami model such as neglecting the wave dispersion and wave breaking as well as to uncertainties in the historical data. It is reasonable that the application of more sophisticated tsunami models could partially reduce some of these discrepancies.

Altogether, the achieved results are satisfying, thus suggesting a reliable back-analysis of the combined landslide-tsunami event. We can conclude that if the simulation of landslide is supported by good input data, collected through detailed investigation, it can be used in the hazard assessment of rock landslide-generated tsunamis. Furthermore, the results confirm the high tsunamigenic potential related to coastal landslides starting at sea level. In fact, these landslides experience an acceleration phase in the first part of the submerged path, thus maintaining Froude number values close to the critical value ($Fr \approx 1$), resulting in highly effective tsunami generation.

Acknowledgments A significant part of the work described in this paper was done while the first author was a guest researcher at the International Centre for Geohazards (Oslo, Norway). ICG-NGI researchers (Unni Eidsvig, Carl Harbitz, Sylfest Glimsdal and Finn Løvholt) performed the numerical modelling of the tsunami and they gave a fundamental support to the revision of the whole paper. Hence, their support is particularly acknowledged. Authors wish to thank Francesco Latino Chiocci and his research team for collecting submarine data and for the constant and fundamental support. A special thanks to the Guest Editor (A. Cattaneo) for the meticulous revision of the paper and the several comments which contributed to a significant improvement of the paper. This research was funded by the PRIN2006 Italian National project “Integration of inshore and offshore geological and geophysical innovative techniques for coastal landslides studies” (Principal Investigator: F.L. Chiocci), Research Unit: “The engineering-geology model as a tool for the dimensioning of gravity-induced coastal instabilities” (Associated Investigator: F. Bozzano).

References

- Baratta M (1901) I Terremoti d’Italia. Saggio di Storia, Geografia e Bibliografia Sismica Italiana, F.Ili Bocca, Turin, Italy (in Italian)
- Baratta M (1910) La catastrofe sismica calabro-messinese (28 dicembre 1908). Rend Soc Geogr It 496 (in Italian)
- Boschi E, Guidoboni E, Ferrari G, Mariotti D, Valensise G, Gasperini P (2000) Catalogue of strong Italian earthquakes from 461 b.C. to 1997. Ann Geofis 43:609–868
- Bosman A, Bozzano F, Chiocci FL, Mazzanti P (2006) The 1783 Scilla tsunami: evidences of a submarine landslide as a possible (con?)cause. EGU 2006, Geophysical Research Abstracts, 8, p 10558
- Bozzano F, Gaeta M, Martino S, Mazzanti P, Montagna A, Prestininzi A (2008) The 1783 Scilla rock avalanche (Calabria, Southern Italy). In: Chen Z, Zhang J, Li Z, Wu F, Ho K (eds) Proceeding of the 10th international symposium on landslides and engineered slopes, 30 June–4 July 2008, Xi’an (China), vol II. Taylor and Francis Group, London, pp 1381–1387
- Bozzano F, Esposito E, Lenti L, Martino S, Montagna A, Paciello A, Porfido S (2010) Numerical modelling of earthquake-induced rock landslides: the 1783 Scilla case-history (Southern Italy). In:

- Fifth int. conf. on recent advances in earthquake engineering and soil dynamics, 24–29 May 2010, San Diego, California, Paper n.4.2b
- De Lorenzo A (1877) Memorie da servire alla storia sacra e civile di Reggio e delle Calabrie, Cronache e Documenti inediti o rari, vol I, Reggio Calabria
- Evans SG, Tutubalina OV, Drobyshev VN, Chernomorets SS, McDougall S, Petrakov DA, Hungr O (2009) Catastrophic detachment and high-velocity long-runout flow of Kolka Glacier, Caucasus Mountains, Russia in 2002. *Geomorphology* 105: 314–321
- Gerardi F, Barbano MS, De Martini PM, Pantosti D (2008) Discrimination of tsunami sources (Earthquake versus Landslide) on the basis of historical data in Eastern Sicily and Southern Calabria. *Bull Seismol Soc Am* 98(6):2795–2805
- Graziani L, Maramai A, Tinti S (2006) A revision of the 1783–1784 Calabrian (southern Italy) tsunamis. *Nat Hazards Earth Syst Sci* 6:1053–1060
- Hamilton W (1783) Relazione dell’ultimo terremoto delle Calabrie e delle Sicilia, sent by Hamilton SEG (trans: doctor Sella, G, Firenze)
- Harbitz CB (1992) Model simulations of tsunamis generated by the Storegga slide. *Mar Geol* 105:1–21
- Harbitz C, Pedersen G (1992) Model theory and large water waves, due to landslides. Preprint Series, 4, Department of Mathematics, University of Oslo
- Harbitz CB, Pedersen G, Gjevik B (1993) Numerical simulations of large water waves due to landslides. *J Hydraul Eng* 119: 1325–1342
- Harbitz CB, Løvholt F, Pedersen G, Masson DG (2006) Mechanisms of tsunami generation by submarine landslides: a short review. *Nor J Geol* 86:255–264
- Hungr O (1995) A model for the runout analysis of rapid flow slides, debris flows, and avalanches. *Can Geotech J* 32:610–623
- Hungr O, Evans SG (1996) Rock avalanche runout prediction using a dynamic model. In: Senneset K (eds) Proc. 7th. international symposium on landslides, Trondheim, Norway, 1. pp 233–238
- Hungr O, McDougall S (2009) Two numerical models for landslide dynamic analysis. *Comput Geosci* 35:978–992
- Locat J, Lee HJ, Locat P, Imran J (2004) Numerical analysis of the mobility of the Palos Verdes debris avalanche, California, and its implication for the generation of tsunamis. *Mar Geol* 203: 269–280
- Løvholt F, Harbitz CB, Haugen KB (2005) A parametric study of tsunamis generated by submarine slides in the Ormen Lange/Storegga area off Norway. *Mar Petroleum Geol* 22:219–231
- Mangeney A, Heinrich P, Roche R, Boudon G, Cheminée JL (2000) Modeling of debris avalanche and generated water waves: application to real and potential events in Montserrat. *Phys Chem Earth* 25(9–11):741–745
- Mazzanti P (2008a) Studio integrato subaereo-subacqueo di frane in ambiente costiero: i casi di Scilla (RC) e del lago di Albano (RM). *Giornale di Geologia Applicata* 8(2):245–261
- Mazzanti P (2008b) Analysis and modelling of coastal landslides and induced tsunamis. PhD Thesis “Sapienza” University of Rome, Department of Earth Sciences
- Mazzanti P, Bozzano F (2009) An equivalent fluid/equivalent medium approach for the numerical simulation of coastal landslide’s propagation: theory and case studies. *Nat Hazards Earth Syst Sci* 9:1941–1952
- Mazzanti P, Bozzano F, Avolio MV, Lupiano V, Di Gregorio S (2009) 3D numerical modelling of submerged and coastal landslides’ propagation. In: Mosher DC, Shipp C, Moscardelli L, Chaytor J, Baxter C, Lee H, Urgeles R (eds) Submarine mass movements and their consequences IV advances in natural and technological hazards research, vol 28. Springer, The Netherlands, pp 127–139
- McDougall S, Hungr O (2004) A model for the analysis of rapid landslide motion across three-dimensional terrain. *Can Geotech J* 41:1084–1097
- McDougall S, Boulbee N, Hungr O, Stead D, Schwab JW (2006) The Zymoetz River landslide, British Columbia, Canada: description and dynamic analysis of a rock slide–debris flow. *Landslides* 3:195–204
- Mercalli G (1906) Alcuni risultati ottenuti dallo studio del terremoto calabrese dell’ 8 settembre 1905. *Atti dell’Accademia Pontoniana di Napoli* 36:1–9
- Minasi G (1785) Continuazione ed appendice sopra i tremuoti descritti nella relazione 468 colla data di Scilla de 30 settembre 1783 con altro che accadde in progresso, 469 Messina
- Minasi A (1970) La specola del filosofo, Natura e sorti nelle incisioni di Antonio Minasi, Ilario Principe, “Brutium”
- Mohrig D, Whipple K, Ellis C, Parker G (1998) Hydroplaining of subaqueous debris flows. *Geol Soc Am Bull* 110:387–394
- Monaghan JJ (1992) Smoothed particle hydrodynamics. *Annu Rev Astron Astrophys* 30:543–574
- NGI (2008) Semi-annual report: tsunami impact in the outer part of Storfjorden, testing of numerical models for rock slide and tsunami, coupling to laboratory experiments. NGI report 2005 1018-2
- Okal EA, Synolakis CE (2004) Source discriminants for near-field tsunamis. *Geophys J Int* 158:899–912
- Pedersen G, Gjevik B (1983) Run-up of solitary waves. *J Fluid Mech* 135:283–299
- Pirulli M, Mangeney A (2008) Results of back-analysis of the propagation of rock avalanches as a function of the assumed rheology. *Rock Mech Rock Eng* 41(1):59–84
- Sarconi M (1784) Istoria de’ fenomeni del tremuoto avvenuto nelle Calabrie, e nel Valdemone nell’anno 1783. Reale Accademia delle Scienze, e delle Belle Lettere di Napoli, Napoli
- Sosio R, Crosta GB, Hungr O (2008) Complete dynamic modelling calibration for the Thurwieser rock avalanche (Italian Central Alps). *Eng Geol* 100:11–26
- Tinti S, Guidoboni E (1988) Revision of the tsunamis occurred in 1783 In Calabria and Sicily (Italy). *Sci Tsunami Hazards* 6(1):17–22
- Tinti S, Maramai A, Graziani L (2004) The new catalogue of Italian tsunamis. *Nat Hazards* 33:439–465
- Tinti S, Maramai A, Graziani L (2007) The Italian Tsunami Catalogue (ITC), Version 2. <http://www.ingv.it/servizi-e-risorse/BD/catalogo-tsunami/catalogo-degli-tsunami-italiani>
- Vivenzio G (1788) Istoria de’ tremuoti avvenuti nella provincia di Calabria ulteriore e nella città di Messina nell’anno 1783, Napoli